Applied Geochemistry 116 (2020) 104580

Contents lists available at ScienceDirect

Applied Geochemistry

journal homepage: http://www.elsevier.com/locate/apgeochem

Retention of technetium-99 by grout and backfill cements: Implications for the safe disposal of radioactive waste

Matthew Isaacs [a,b], Steve Lange [b], Guido Deissmann [b], Dirk Bosbach [b], Antoni E. Milodowski [a,c], David Read [a,d,*]

[a] Department of Chemistry, University of Surrey, Guildford, GU2 7XH, United Kingdom
[b] Institute of Energy and Climate Research (IEK-6): Nuclear Waste Management and Reactor Safety, Forschungszentrum Jülich GmbH, 52425, Jülich, Germany
[c] British Geological Survey, Keyworth, Nottingham, NG12 5GG, United Kingdom
[d] National Physical Laboratory, Hampton Road, Teddington, Middlesex, TW11 0LW, United Kingdom

ARTICLE INFO

Keywords:
Technetium
Adsorption
Diffusion
Cement

ABSTRACT

Technetium-99 (^{99}Tc) is an important radionuclide when considering the disposal of nuclear wastes owing to its long half-life and environmental mobility in the pertechnetate (Tc(VII)) redox state. Its behaviour in a range of potential cement encapsulants and backfill materials has been studied by analysing uptake onto pure cement phases and hardened cement pastes. Preferential, but limited, uptake of pertechnetate was observed on iron-free, calcium silicate hydrates (C–S–H) and aluminate ferrite monosulphate (AFm) phases with no significant adsorption onto ettringite or calcium aluminates. Diffusion of ^{99}Tc through cured monolithic samples, representative of cements being considered for use in geological disposal facilities across Europe, revealed markedly diverse migration behaviour, primarily due to chemical interactions with the cement matrix rather than differential permeability or other physical factors. A backfill cement, developed specifically for the purpose of radionuclide retention, gave the poorest performance of all formulations studied in terms of both transport rates and overall technetium retention. Two of the matrices, pulverised fuel ash: ordinary Portland cement (PFA:OPC) and a low-pH blend incorporating fly ash, effectively retarded ^{99}Tc migration via precipitation in narrow, reactive zones. These findings have important implications when choosing cementitious grouts and/or backfill for Tc-containing radioactive wastes.

1. Introduction

Technetium-99 (^{99}Tc) is a low energy (E_{max} = 0.29 MeV), beta-emitting product of uranium fission in a nuclear reactor. It is also produced, in smaller quantities, from isomeric transition of the diagnostic nuclear medicine isotope ^{99m}Tc. Given its long half-life (211,100 years; Brown et al., 2018), high yield (6.1% for thermal neutron fission of ^{235}U; Brown et al., 2018) and environmental mobility (Wildung et al., 1978; Schulte and Scoppa, 1987; Lloyd et al., 2000; Masters-Waage et al., 2017), retention of ^{99}Tc is an important factor to consider when assessing the safety performance of radioactive waste repositories. In addition to its occurrence as a fission product in spent nuclear fuels (Kleykamp, 1988; Bruno and Ewing, 2006; Carbol et al., 2012; Lewis et al., 2012), it typically occurs in operational wastes such as ion-exchange resins, contaminated liquids, filters and sludge (Westsik et al., 2014; Ochs et al., 2016) and therefore, some form of treatment is required to render it into a passive, solid waste form. Cement is the most commonly used encapsulant for reasons of cost or ready availability and also because the behaviour of technetium during high-temperature thermal treatment such as vitrification is problematic; it volatiles and only a fraction is retained in the glass (e.g. Childs et al., 2015; Pegg, 2015; Luksic et al., 2015; Kim and Kruger, 2018). Unfortunately however, data on the interactions of technetium with cementitious phases and hardened cement pastes (HCP) is limited.

Retardation of radionuclides in cement can occur by three principal mechanisms; precipitation of insoluble phases, incorporation into existing or newly-formed mineral phases and surface adsorption (Jantzen et al., 2010; Westsik et al., 2014; Ochs et al., 2016). Thus, the capacity of a cement grout or backfill to retain any given radionuclide will vary depending on the chemical speciation of the nuclide and the properties of the cement. The potential for precipitation of cationic species in high pH cementitious pore waters is well known: similarly,

* Corresponding author. Department of Chemistry, University of Surrey, Guildford, GU2 7XH, United Kingdom.
E-mail address: d.read@surrey.ac.uk (D. Read).

https://doi.org/10.1016/j.apgeochem.2020.104580
Received 4 October 2019; Received in revised form 27 February 2020; Accepted 23 March 2020
Available online 2 April 2020

uptake in cementitious systems by adsorption to calcium silicate hydrate (C–S–H) phases, uptake into the C–S–H interlayer, exchange of Ca ions in the C–S–H structure or incorporation into layered double hydroxide (LDH)-type phases, such as AFm, (e.g. Atkins et al., 1992; Evans, 2008; Ochs et al., 2016). However, it is often assumed, at least in safety assessments, that anionic species will be much more mobile (e.g. Posiva, 2012; SKB, 2015). Recent research has challenged this assumption by demonstrating the precipitation and/or mineralisation of selenium (Felipe-Sotelo et al., 2016a), chlorine (Milodowski et al., 2013; van Es et al., 2015) and iodine (Felipe-Sotelo et al., 2014). Moreover, redox-sensitive, anionic radionuclides of, for example, selenium or technetium, may be precipitated in less soluble, reduced forms, depending on conditions, e.g. in slag-rich formulations. Nevertheless, retention of anionic species has not been studied to the same extent as cations and there is no guarantee that findings for ordinary Portland cement (OPC) will be valid for the wide variety of blended cement formulations under consideration in nuclear waste management. Changes associated with degradation of the cement matrix over time and the presence of additives such as superplasticisers further complicate the issue (Ochs et al., 2016; Isaacs et al., 2018).

Technetium is a redox sensitive element and can occur in nuclear waste streams in either the Tc(IV) or Tc(VII) state, depending on the redox potential of the solution and pH (Fig. 1). Speciation calculations suggest that its solubility will be in the range 10^{-7} - 10^{-6} mol dm^{-3}, controlled by hydrous TcO_2, in the presence of corroding iron from steel drums (Eh ~ - 800 mV) and over the pH range anticipated for cementitious conditions. Irrespective of the redox state, dissolved Tc in cementitious environments will be present predominantly in an anionic form either as $TcO(OH)_3^-$ or as TcO_4^-; the pertechnetate ion (TcO_4^-) is favoured under more oxidising and also hyper-alkaline conditions (Eriksen et al., 1993; Cui and Eriksen, 1996; Burke et al., 2005; Warwick et al., 2007; Hallam et al., 2011).

Previous studies indicate that pertechnetate is poorly retained in both young and mature Portland cements due to the negatively charged surfaces of C–S–H (Tallent et al., 1987; Brodda and Xu, 1989; Smith and Walton, 1993; Mattigod et al., 2001, 2004; Evans, 2008; Corkhill et al., 2012). The major mechanism of retention of technetium in blended cements was found to be reduction to less mobile Tc(IV) or Tc(0) by reducing agents present in those materials. Tallent et al. (1987) studied the influence of grout composition on the leachability of technetium-containing cementitious matrices. They demonstrated that leachability decreases with increasing mix ratio, grout fluid density and blast furnace slag (BFS) content. Later, Gilliam et al. (1990) showed that

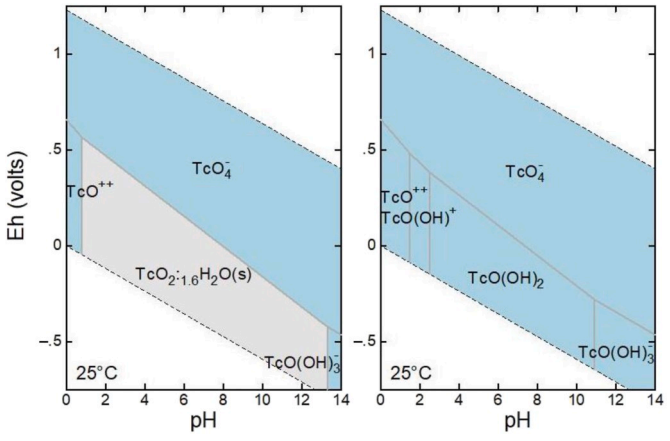

Fig. 1. Eh-pH diagram for Tc species in aqueous systems (Tc = 10^{-6} M(left), Tc = 10^{-9} M(right). Aqueous species are shown in light blue, solids in light grey. Thermodynamic database: ThermoChimie Version 9b0; Giffaut et al., 2014; Grivé et al., 2015). (For interpretation of the references to colour in this figure legend, the reader is referred to the Web version of this article.)

the effective technetium diffusivity of cement-based waste forms decreases by five orders of magnitude on the addition of BFS. A further decrease of the leach coefficient in water and brine was achieved by addition of sodium sulphide, as reported by Brodda and Xu (1989), who concluded that technetium appeared to be chemically bound. Thermodynamic calculations carried out by Smith and Walton (1993) suggested that technetium leachability decreases owing to reaction with the sulphur present in BFS and formation of Tc_2S_7. The addition of a limited amount of BFS led to a significant improvement in leach test performance but further BFS loading had only a marginal effect.

Allen et al. (1997a,b) conducted extended X-ray absorption fine structure (EXAFS) studies on the effect of blast furnace slag and metal sulphides on technetium speciation. Their results demonstrated that the addition of BFS to a cement formulation leads to only partial reduction of any pertechnetate anions present, whereas the addition of Na_2S or FeS results in complete reduction to the less mobile Tc(IV). They concluded that sulphide-containing species rather than elemental sulphur are the active reducing agents in BFS. These authors also measured interatomic Tc–S and Tc–Tc distances in the presence of Na_2S or FeS, observing bond distances in agreement with an oligomeric structure similar to that found in TcS_2 (Allen et al., 1997a, b).

Not all authors agree that reduction to Tc(IV) is necessary for technetium immobilisation. Berner (1999) suggested that binding and/or incorporation of TcO_4^- into the alumina ferric mono/tri-sulphate (AFm/AFt) phases of cement systems could also be expected, by analogy to other oxo-anions such as SO_4^{2-} or MoO_4^{2-}, and possibly also SeO_3^{2-}. This has been tentatively confirmed in the case of ettringite by EXAFS and X-ray absorption near edge structure (XANES) analysis of a hydrated lime and sulphate-rich simulant waste form (Saslow et al., 2018). The resulting spectra show that TcO_4^- substitutes directly for sulphate in the crystal lattice. The findings imply reduction to Tc(IV) is not essential for technetium immobilisation, which is important as oxygen diffusion and re-oxidation of Tc(IV) in a waste form might occur over longer timescales. Indeed, Smith and Walton (1993) concluded that the diffusion of oxygen into HCP or concrete would oxidise Tc_2S_7 to the highly mobile TcO_4^-, which could then diffuse out from the waste.

Layered double hydroxides have also been suggested as potential host phases for technetium in its anionic form. Several natural minerals are known to incorporate technetium, for example fougerite (green rust), a layered double hydroxide-carbonate belonging to the hydrotalcite group, with the formula $([Fe^{2+}{}_4Fe^{3+}{}_2(OH)_{12}][CO_3]{\cdot}3H_2O)$, as well as potassium metal sulphides. A good overview of these potential host phases is given by Luksic et al. (2015).

Finally, some radioactive waste disposal concepts are considering cements not only as grouts but as potentially suitable backfill materials and as a component in specific high-level waste containers (e.g. Bel et al., 2006; NAGRA, 2002, 2008; Verhoef et al., 2014). Clearly, the situation where the cementitious barrier is already in place before encountering migrating radionuclide species is very different from the intimate mixing of unhydrated cement pastes with aqueous wastes. The aim of the present work is to assess both situations by considering the uptake of ^{99}Tc in a) a number of individual cement phases and HCP and b) diffusion of ^{99}Tc through cured monolithic samples representative of those being considered for use in geological disposal facilities across Europe.

2. Experimental

The solids of interest fall into two categories, single cement mineral phases and hardened cement pastes (HCP); both were used for batch adsorption tests with the latter also employed for through-diffusion studies. Cement minerals comprised C–S–H with calcium: silica ratios of 0.9 and 1.4 (denoted C–S–H0.9 and C–S–H1.4, respectively), ettringite (AFt, $Ca_6Al_2(SO_4)_3(OH)_{12}{\cdot}26H_2O$), hydrogarnet (C3AH6, $Ca_3Al_2(OH)_{12}$), portlandite ($Ca(OH)_2$), calcite ($CaCO_3$) and two AFm phases ($Ca_4Al_2(OH)_{12}$ $(X^{2-}){\cdot}6H_2O$) namely, AFm-SO_4 and AFm-CO_3. The

synthesis of these model phases, representative of hydration products in HCP, were carried out following established procedures (i.e. C–S–H: Atkins et al., 1992; AFm: Baur et al., 2004 and Matschei et al., 2006; ettringite: Atkins et al., 1991 and Baur et al., 2004). The methods are described in detail in Lange et al. (2018). In order to avoid carbonation of the material, synthesis of the phases, sample preparation and storage were carried out in an argon glove box (<10 ppm CO_2). After purification, structure and purity of the model phases as well as the phase assemblages present in HCP samples were characterised by powder X-ray diffraction spectroscopy (XRD), using either a D8 Advance (Bruker AXS GmbH) with a θ-θ geometry or a D4 Endeavor (Bruker AXS GmbH) with a θ-2θ geometry, employing CuK_α-radiation. Microstructure and phase morphology were investigated by Scanning Electron Microscopy (SEM; FEI Quanta 200F) equipped with a field emission cathode. Energy dispersive X-ray spectroscopy (EDX) was performed using an Apollo X Silicon Drift Detector (SDD) from EDAX. SEM/EDX analyses were carried out in low vacuum mode (60 Pa) to avoid coating the samples with carbon or gold. The characteristics of the phases are described in detail elsewhere (Lange et al., 2018).

Sorption distribution ratios (R_d values) and technetium uptake kinetics on the model phases were determined in static batch experiments under anoxic conditions, employing different test solutions. Generally, 20 cm^3 LDPE bottles were used at solid to liquid (S/L) ratios of 0.005–0.04 kg dm^{-3}, depending on the aim of experiment. In the first set of experiments, weighed amounts of dried solids were equilibrated with deionised water (18.2 MΩ) to obtain equilibrium solutions (ES); the suspensions were stored at room temperature for up to 14 days under anoxic conditions to achieve equilibrium between aqueous and solid phases. Subsequently, solid and liquid phases were separated by filtration. The pH of the respective equilibrium solutions is provided in Table S1 in the Supplementary Information. pH measurements were performed with a Metrohm Unitrode electrode with integrated Pt-temperature sensor, suitable for measurements between pH 0 and 14. In addition to solutions equilibrated with the respective solids, experiments using an alkali-rich artificial young cement water (ACW, pH > 13) and a solution saturated with portlandite (CH, pH ~12.5) were performed to address conditions representative of concrete degradation stages I and II (Glasser, 2011; Hoch et al., 2012; Ochs et al., 2016). Artificial young cement water was prepared by filtration and dilution of highly concentrated sodium and potassium hydroxide solutions, subsequently saturated with $Ca(OH)_2$ (Wieland et al., 1998). The resulting solution containing 0.114 mol dm^{-3} Na and 0.18 mol dm^{-3} K had a pH of 13.3; the saturated portlandite solution (CH) contained 0.19 mol dm^{-3} Ca at pH 12.3.

For the sorption experiments, defined amounts of the respective fresh model phases were added to the equilibrium solutions at a S/L-ratio of 0.04 kg dm^{-3} and stored for an additional 14 days, before ^{99}Tc was added as a tracer in the form of pertechnetate at concentrations ranging from 10^{-5} M to 10^{-7} M. Solution activity concentrations were monitored for up to 100 days by liquid scintillation counting (LSC) to ensure steady state had been reached; the bottles were shaken by hand regularly. To avoid removing solution during sampling, a separate test batch was used for each time step in those experiments addressing uptake kinetics. The pH in the respective solutions was found to be constant over the duration of the experiments. The timeframes for experiments to determine final R_d values were defined based on the uptake kinetics. Adsorption of pertechnetate to reaction vessels and filters was tested prior to the experiments and found to be negligible.

LSC measurements were performed using a 1220 Ultra low level Quantulus™ LSC device (Perkin Elmer). Sample aliquots of 50 μL were diluted in a 20 cm^3 polyethylene vial with 15 cm^3 Hionic-Fluor or Ultima Gold™ LSC-cocktail (Perkin Elmer). Liquid and solid phases were separated using USY-1 ultrafilters (10,000 Da, Advantec) prior to analysis of the concentration in solution. At the end of the batch sorption experiments the solids were separated by filtration and analysed by XRD and SEM-EDX.

The uptake of technetium by the solid phases is described here in terms of a distribution ratio R_d between ^{99}Tc adsorbed by the solids ($^{99}Tc_{sorbed}$) and the ^{99}Tc remaining in solution ($^{99}Tc_{solution}$) as:

$$R_d = \frac{^{99}Tc_{sorbed}}{^{99}Tc_{solution}} \quad \text{(eq. 1)}$$

and calculated according to:

$$R_d = \frac{^{99}Tc_{initial} - ^{99}Tc_t}{^{99}Tc_t}\frac{V}{m} \quad \text{(eq. 2)}$$

where $^{99}Tc_{initial}$ is the initial concentration of ^{99}Tc in solution (Bq or M), and $^{99}Tc_t$ the concentration at time t, respectively; V is the volume of the liquid phase and m the mass of solid used in the experiment. Estimation of uncertainties for the distribution ratio (R_d) was performed using the statistical software of the LSC device, comprising uncertainties resulting from both the sample measurement and the background spectra. Errors arising from each step of the experimental procedure (e.g. weighing and pipetting) were included using Gaussian error propagation.

Similar batch experiments were carried out on two HCP samples, CEM I and a low-pH reference cement blend used for benchmarking purposes in the pan-European CEBAMA project (Grambow et al., 2020), produced according to a specification provided by Valtion Teknillinen Tutkimuskeskus (VTT), Finland (Vehmas et al., 2017, Vehmas et al., 2020). CEM I HCP specimens were prepared in a glove box under argon atmosphere (<10 ppm CO_2), using a commercially available Portland cement (CEM I 32.5 R; Heidelberger Zement) at a water/cement ratio (w/c) of 0.4 dm^3 kg^{-1}. The cement pastes were cast in cylindrical moulds and cured for at least 28 days submerged in water under anoxic conditions; the demoulded monoliths were subsequently stored under argon atmosphere. In addition to OPC, the Cebama reference blend low pH cement formulation comprised blast furnace slag and silica fume as well as quartz filler (Vehmas et al., 2017; *cf*. Table 2). This HCP, provided by VTT, had been prepared with a w/c-ratio of 0.25 dm^3 kg^{-1} and hydrated for 90 days in a saturated KOH solution to prevent leaching. The HCP was mechanically crushed, followed by multipoint N_2-BET surface area determination, using a Quantachrome Autosorb 1. Adsorption experiments with HCP were performed in an analogous manner to the experiments with model phases at a S/L-ratio of 0.02 kg dm^{-3}, using crushed materials in solutions pre-equilibrated for 14 days with the respective HCP. The pH of the equilibrated solutions used in the experiments was 12.6 (CEM I) and 12.5 (Cebama low-pH reference blend), respectively. The rather low equilibrium pH in the system with crushed CEM I HCP in comparison to the pH expected in young Portland cement-based systems is attributed to the low S/L-ratio used in the experiments and thus, the low alkali inventory.

Five cement blends were included in the through-diffusion study; an ordinary Portland cement (OPC; CEM I), a ground granulated blast furnace slag: ordinary Portland cement blend (GGBS:OPC), a pulverised fuel ash blend (PFA:OPC), a bespoke backfill material (NRVB, Nirex Reference Vault Backfill) and the reference cement blend used for benchmarking purposes noted above, provided by VTT, Finland (Vehmas et al., 2017, 2020).

The CEM I 42.5N, obtained from Hanson Cement, Ribblesdale, UK with a fineness of 347 m^2 kg^{-1} and specific gravity of 3.13 g cm^{-3}, complies with both BS EN 197–1:2011 and a technical specification (Angus et al., 2011) for the supply of powders for the encapsulation of intermediate level radioactive waste (ILW) in the UK. The GGBS, with fineness of 517 m^2 kg^{-1} and specific gravity of 2.91 g cm^{-3}, was obtained from Hanson Cement, Scunthorpe, UK (Isaacs et al., 2018); it complies with BS EN 15167–1:2006. Hydrated lime (Lafarge) complies with the requirement of BS EN 459-1 to be building lime standard. Limestone flour is available commercially (NAF Limestone Flour, NAF, Monmouth, UK). The constituents of the Cebama reference blend were provided by VTT, as noted above. The Finnish CEM I (Cementa) has a fineness of 310

m^2 kg^{-1} and complies with the EN 197-1 standard. Finnish GGBS (Finnsementti) has a fineness of ≥275 m^2 kg^{-1} and meets the technical specification of EN 15167–1:2006. Silica fume was also derived from Finnsementti and meets the standard of EN 13263–1:2009. The water/cement ratio was increased slightly from that specified by VTT to provide a workable cement in the absence of plasticiser (Isaacs et al., 2018).

X-ray fluorescence (XRF) analysis was used to determine the major components of these starting materials (Table 1). The formulations used for each of the HCP samples are detailed in Table 2.

The powders were mixed using a bench-top conical mixer in a polypropylene hexagonal barrel (Pascall Lab-mixer II, Pascall Engineering) until homogeneous. A series of pre-equilibrated waters for use in the experiments was prepared by adding 50 g of each HCP powder above to 1 dm^3 deionised water under N_2 atmosphere. The suspension was agitated daily to prevent sedimentation. After 28 days the solids were removed by filtration and the solutions analysed by ion chromatography (Table 3).

An aliquot of pre-equilibrated solution was added to each HCP powder at a liquid/solid ratio of 0.45 and mixed for 5 min by hand. The mix was then poured into 50 cm^3 polypropylene containers, gently tapped to remove any trapped air bubbles and left to set for 24 h before removing the cylinders from the moulds. The samples were cured in sealed containers for a period of 28 days before use in the diffusion experiments. After the curing period, the blocks were removed from the solution and a well drilled centrally along the longitudinal axis of the cylinders; the depth of the central well was 30 mm with a diameter of 10 mm. The top and bottom surfaces of the block were sealed with wax. The cement cylinders had a diameter of 40 mm and a length of 40–45 mm.

The diffusion of ^{99}Tc through cured HCP samples was assessed using an experimental protocol described previously (Felipe-Sotelo et al., 2014, 2016a,b; van Es et al., 2015). An aliquot of ^{99}Tc (1.6 kBq) as ammonium pertechnetate in 1 cm^3 pre-equilibrated cement water was spiked into the central well of the block, which was then sealed and submerged in 200 cm^3 of the same pre-equilibrated water used for curing (Fig. 2). The cement blocks, sealed in individual Nalgene containers, were kept in a N_2-atmosphere glove box throughout the experiment and during sampling. All experiments were carried out in duplicate.

Movement of ^{99}Tc through the block was monitored by measuring the equilibrated water surrounding the block by taking 1 cm^3 aliquots initially on a daily basis and then weekly. The solutions were filtered before use through qualitative filter paper (Fisher Scientific). The activity in the samples was determined by LSC (Packard 2100 TR, Liquid Scintillation Analyzer) in the energy range between 20 and 200 keV after the addition of liquid scintillation cocktail (Goldstar, Meridian, UK) at a sample to scintillant ratio of 1:10. Each sample was agitated on a whirlimixer for 30 s and the samples were stored in a dark room for a minimum of 24 h before measurement.

At the end of the equilibration period, the cylinders were removed from solution and cut longitudinally with a diamond masonry saw in order to determine the migration profiles of the ^{99}Tc by digital laser-photostimulated luminescence (LPSL) autoradiography, using storage phosphor imaging plates (IP). The IP comprise a layer of microcrystalline Eu-doped barium fluorobromide (BaFBr:Eu^{2+}) photo-stimulable phosphor layer bonded to a polyester plastic support. Incident radiation excites Eu^{2+} from its ground state to the metastable Eu^{3+}, liberating electrons to the conduction band, which are trapped in crystal defects (hole-electron pairs or F-centres) in proportion to the incident radiation (Zeissler, 1997; Gonzalez et al., 2002; Takahashi, 2002; Leblans et al., 2011). Stimulation of the phosphor by red laser light excites the stored electrons to the conduction band, where they recombine with Eu^{3+} ions, releasing energy in the form of blue light as a result of 5d-4f transition when the excited electron falls to the ground state in the Eu^{2+} ion. This emitted light is detected by a photomultiplier and is proportional to the radioactivity that the phosphor was exposed to (Takahashi, 2002; Leblans et al., 2011). The IP technique cumulatively detects alpha-, beta- and gamma-radiation, as well as background cosmic radiation.

The IP were initially exposed to bright white fluorescent light for 20 min to erase any previously-acquired residual latent image and background (gamma and cosmic) radiation signal. LPSL autoradiography images were produced by placing the flat surfaces of the cut cylinders directly onto Fuji BAS-MP2025P general purpose polyurethane-coated IP for 4 h in a light-tight box. Following exposure, the IP were carefully removed under darkroom conditions and scanned using an Amersham Biosciences (GE Healthcare Ltd) STORM™ 860 digital fluorescence laser scanner, with red laser light (635 nm) and a 650 nm low-pass wavelength filter, to release the stored energy and record the latent image. The IP were scanned at a 50 μm pixel resolution and the resultant digital autoradiography images were recorded as 16-bit 'GEL-format' image files. These employ a square root algorithm coupled with a 'scaling factor' to accommodate the wide dynamic range of the IP, and compresses the 100,000 possible levels of signal resolution into the more limited range available in a standard TIFF (tagged image file) image. This provides higher signal resolution at the low end where changes in signal are more critical. However, the resulting raw data stored within each pixel of a GEL image file are non-linear. The 'GEL-format' LPSL autoradiography images were initially processed using the ImageQuant TL (v.2005) software package (Amersham Biosciences, 2005). The GEL files were subsequently processed to produce detailed, 16-level colour-contoured autoradiographs using the FiJi (ImageJ) (v. 1.48k 15 December 2013) public-domain open-source software package (Rasband, 2013). This was coupled with the 'Linearise GelData' software 'plug-in' (Cathelin, 2012) to square and scale the GEL file data (default scale factor for 'GEL-format' files is 1/21025) in order for the images to be displayed correctly as quantitative linear colour-contoured intensity images. ImageQuant TL (v.2005) was also used to plot the variation in radioactivity (determined as image 'diffuse density') across the cement blocks from the LPSL autoradiography images, along 'lane profiles' drawn perpendicular to the walls of the well.

For comparison purposes, similar experiments were carried out for each HCP formulation using a nominally conservative tracer, tritiated water (HTO). A total activity of approximately 5000 Bq (Perkin Elmer) was added to the central well of the cement blocks. As for the technetium experiments, HTO diffusion was assessed in duplicate and breakthrough was determined by LSC.

Table 1
Major elements in the constituents used to prepare the cement pastes for through-diffusion experiments.

Cement Powder	CaO [wt%]	SiO_2 [wt%]	Al_2O_3 [wt%]	SO_3 [wt%]	MgO [wt%]	Fe_2O_3 [wt%]	K_2O [wt%]	P_2O_5 [wt%]	TiO_2 [wt%]	MnO [wt%]
CEM I	66.27	17.86	4.78	3.98	2.75	2.65	1.52	nd	0.2	nd
PFA	3.86	48.66	25.97	1.82	1.27	12.36	5.05	0.18	0.84	nd
GGBS	42.93	31.92	11.40	4.10	6.76	0.45	1.01	nd	0.41	0.59
Hydrated Lime	97.75	1.37	0.35	nd	0.20	nd	0.33	nd	nd	nd
Lime Flour	96.57	1.70	0.71	0.18	0.29	0.16	0.39	nd	nd	nd
Silica Fume	1.46	93.10	1.44	0.47	0.88	0.91	1.73	nd	nd	nd
CEM I (VTT)	67.72	17.60	3.42	3.81	0.6	5.17	1.3	nd	0.17	0.21
GGBS (VTT)	43.13	32.3	9.85	3.68	7.40	0.74	1.20	nd	1.36	0.34

nd – not detected.

Table 2
Formulations of HCP samples used in the through-diffusion experiments.

Cement Blend	OPC	PFA	GGBS	Hydrated Lime	Lime Flour	Silica Fume	Quartz	Water/cement ratio
CEM I	1							0.45
PFA:OPC	1	3						0.45
GGBS:OPC	1		9					0.45
NRVB	1			0.38	1.1			0.55
Cebama	1		0.62			1.05	1.1	0.45

Table 3
Composition of aqueous solutions equilibrated with the HCP used in the through-diffusion experiments.

Cement Blend	Cl mg kg^{-1}	SO_4 mg kg^{-1}	NO_3 mg kg^{-1}	Na mg kg^{-1}	K mg kg^{-1}	Mg mg kg^{-1}	Ca mg kg^{-1}	pH	Eh [mV]
CEM I	18.0	36.9	18.1	267.6	453.3	nd	1388.4	12.8	−14
PFA:OPC	14.4	31.0	16.3	129.8	195.2	39.0	675.8	12.3	−503
GGBS:OPC	16.9	34.7	17.6	68.6	70.2	nd	299.6	12.8	−414
NRVB	16.0	33.6	17.2	172.5	224.7	66.3	1374.3	12.9	−129
Cebama	24.0	50.3	20.4	189.7	202.3	137.0	1046.6	12.7	−454

nd – not detected.

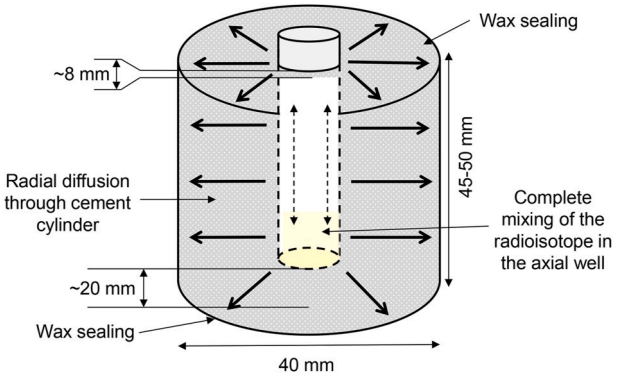

Fig. 2. Schematic of the radial diffusion experiments using various HCP.

3. Results and discussion

3.1. Uptake of ^{99}Tc by individual cement phases

The kinetics of Tc(VII) uptake by the model hydration phases in the various solutions (i.e. with or without alkalis) were determined at a S/L-ratio of 0.005 kg dm^{-3} for up to 100 days; the results of these adsorption tests as a function of time are shown in Fig. S1 in the Supplementary Information. Within experimental error, the measured TcO_4^- concentrations in solution were similar to the initial tracer concentration (10^{-7} M), indicating only minor retention by the pure model phases. Thus, calculated R_d values encompass negative values and could not be distinguished from background. Where uptake was observed, the kinetic tests indicate a fast uptake process, leading to equilibrium within a few days.

Equilibrium R_d values determined after 28 days at a S/L ratio of 0.04 kg dm^{-3} are given in Table 4 and shown graphically in Fig. S2 in the Supplementary Information. Apparent differences in the distribution ratios (R_d = 4.5 dm^3 kg^{-1} for C–S–H0.9 and R_d = 2.3 dm^3 kg^{-1} for the more Ca-rich C–S–H1.4) are small and may not be significant. The sorption of oxyanions such as IO_3^- or MoO_4^- to C–S–H is often attributed to electrostatic adsorption to the C–S–H surface (e.g. Bonhoure et al., 2002; Ochs et al., 2016). Thus, uptake of these anions should increase with increasing Ca/Si ratio in C–S–H, since the zeta potential of C–S–H is zero for Ca/Si = 1.2 and negative at Ca/Si < 1.2. Atkins et al. (1992) also predicted that the increasingly positive surface charge at Ca/Si > 1.2 should result in more pronounced uptake of anions. However in our experiments, the higher affinity of TcO_4^- towards C–S–H with lower

Table 4
Distribution coefficients (R_d) for the uptake of ^{99}Tc by cement hydration phases in various solutions (ES: equilibrium solution; ACW: artificial young cement water (pH 13.3); CH: saturated portlandite solution (pH 12.3)).

Phase	R_d [dm^3 kg^{-1}]		
	ES	ACW	CH
C–S–H 0.9	4.5 ± 2.7	4.1 ± 2.7	na
C–S–H 1.4	2.3 ± 2.4	1.9 ± 2.3	na
AFm-SO_4	4.0 ± 1.9	0.7 ± 1.5	0.6 ± 1.5
AFm-CO_3	2.3 ± 1.7	na	1.1 ± 1.5
Ettringite	0.6 ± 0.9	0.6 ± 0.9	0.6 ± 0.9
Hydrogarnet C3AH6	0.6 ± 1.6	0.6 ± 1.6	1.0 ± 1.7
Portlandite	na	na	1.0 ± 2.2
Calcite	0.6 ± 2.2	na	0.8 ± 2.2

na – not analysed.

Ca/Si-ratio, consistently corroborated by the adsorption isotherms obtained at dissolved TcO_4^- concentrations between 10^{-5} and 10^{-8} M (Fig. 3), does not reflect the trend observed for other anions. Considering

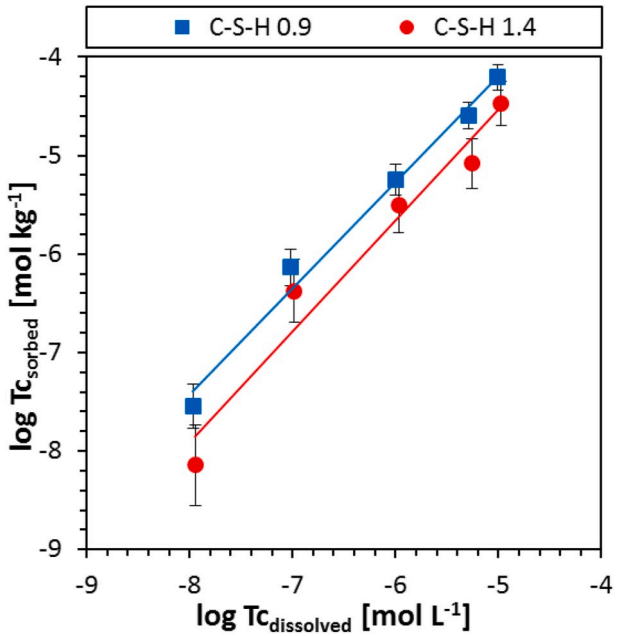

Fig. 3. Sorption isotherms for pertechnetate uptake by C–S–H0.9 and C–S–H1.4.

the generally low distribution ratios obtained, the higher affinity of pertechnetate to C–S–H0.9 might be attributable here to differences in the surface area of the synthetic C–S–H (C–S–H0.9 = 125 m^2 g^{-1}; C–S–H1.4 = 109 m^2 g^{-1}; Lange, 2019). The experiments performed in young cementitious water (ACW) indicated (virtually) no effect of pH and alkali concentration in solution on pertechnetate uptake by the synthesised C–S–H phases.

In addition to C–S–H, some, albeit limited, uptake of pertechnetate was apparent for AFm-SO_4 (R_d = 4.0 dm^3 kg^{-1}) and AFm-CO_3 (R_d = 2.3 dm^3 kg^{-1}). The uptake of the pertechnetate anion by AFm-phases could be due to surface adsorption, edge sorption to the octahedral layers or to exchange for the interlayer anion, similar to the uptake of MoO_4^- or SeO_4^-, as described by Ma et al. (2017, 2019). The potential for anion exchange in the interlayer was probed by XRD measurements, since the size of the pertechnetate oxo-anions (ionic radius of Tc(VII): 37 p.m. for coordination number 4 (Shannon, 1976); Tc–O bond length 173 p.m. (Lukens et al., 2003; Weaver et al., 2017)) is larger than that of sulphate ions (ionic radius of S(VI): 12 p.m. for coordination number 4 (Shannon, 1976); S–O bond length: 147 p.m. (Hawthorne et al., 2000)). However, no changes in the interlayer spacing of the AFm phases or new reflections attributable to the exchange of pertechnetate for the interlayer anions were observed. These findings probably reflect the low degree of uptake of pertechnetate by the AFm phases, bearing in mind that a change in the extent of hydration (i.e. the number of water molecules in the interlayer) accompanying the anion exchange process would also affect the interlayer distance. Generally, for the exchange of interlayer anions in layered double hydroxides and AFm-type phases, divalent anions (e.g. CO_3^{2-} or SO_4^{2-}) are preferred over monovalent anions (e.g. TcO_4^-, Cl^-, IO_3^-, I^-; Jantzen et al., 2010). However, the slightly lower pertechnetate uptake by AFm-CO_3 compared to AFm-SO_4 might indicate that exchange of the (tetrahedral) TcO_4^- for the planar CO_3^{2-}-anion is less favoured compared to exchange with the tetrahedral SO_4^{2-}-anion. The less pronounced pertechnetate uptake by the AFm phases in young cement water and portlandite buffered solutions suggests a slight dependence on solution pH and composition.

The uptake of pertechnetate by all other model phases tested was found to be negligible (Table 4). The R_d value determined for systems containing ettringite was <1 dm^3 kg^{-1}, indicating practically no uptake of TcO_4^- due to exchange for the sulphate groups of this phase. This suggests that the uptake mechanism proposed by Berner (1999) does not contribute to Tc(VII) retention in cementitious systems in the case of pre-existing ettringite. In contrast, a partial incorporation of pertechnetate in ettringite precipitating in the presence of dissolved TcO_4^- ions is to be expected (e.g. Saslow et al., 2018), which would be relevant, for example, with respect to the immobilisation of liquid waste streams by cementation.

3.2. Uptake of ^{99}Tc by HCP

Results of the batch sorption experiments using crushed HCP are shown in Fig. 4. Tc(VII) uptake by HCP reached a steady state after only 1 day with rather low R_d values < 10 dm^3 kg^{-1}. These findings are in good agreement with the stated high mobility and low retention of TcO_4^- in cementitious environments in the absence of reductants (e.g. Ochs et al., 2016). As anticipated from the batch uptake experiments with single phases, the distribution ratios of HCP based on CEM I were somewhat lower than those of the low-pH paste based on the Cebama reference blend. This can be explained by the lower Ca/Si ratio of the C–S–H in the Cebama reference blend HCP, and the higher content of Fe (II) and/or sulphides in this material, due to the GGBS in the cement formulation. The latter could lead to Tc retention by reduction of mobile Tc(VII) to Tc(IV) and consequent formation of TcO_2 or Tc-sulphides (e.g. Allen et al., 1997b; Warwick et al., 2007; Westsik et al., 2014; Masters-Waage et al., 2017).

In experiments using crushed CEM I HCP, the solution pH remained constant throughout (pH ~12.6). Owing to the low S/L-ratio in the experiment and leaching of the alkalis, as indicated by a solution pH probably controlled by portlandite dissolution, the material corresponds to a slightly degraded cement in stage II (Lange et al., 2018). In contrast, with experiments using HCP prepared from the Cebama reference low pH cement blend, the solution pH dropped from an initial 12.5 to 11.8 after 75 days, indicating ongoing hydration of this material. This would lead to continuous formation of C–S–H with low Ca/Si-ratios from remaining unreacted clinker phases (silica fume and blast furnace slag (GGBS)), as predicted by the hydration model of Idiart (2017).

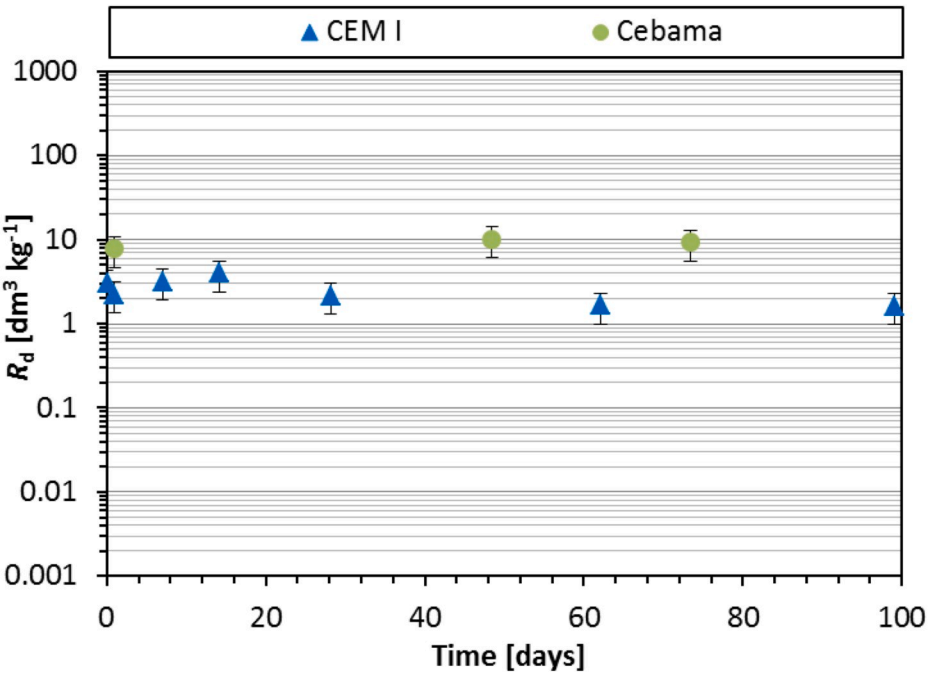

Fig. 4. Uptake kinetics for ^{99}Tc(VII) by HCP made from CEM I and Cebama reference blend.

3.3. Through-diffusion

Retardation of radionuclides by hardened cements reflects a combination of physical and chemical processes. The experiments conducted with tritium represent an attempt to distinguish between the two. This is obviously an over-simplification as, although often regarded as a conservative tracer, tritium will undergo isotopic exchange for hydrogen bound in solid phases, particularly C–S–H and thus, the slower its movement, the greater the scope for interaction; i.e. the physical and chemical aspects are intimately coupled. Nevertheless, the difference in tritium transport rates between respective cement formulations should be, as a first approximation, primarily a function of HCP permeability.

The results demonstrate that initial tritium breakthrough is rapid, as expected, with some ^{3}H detected in the solution surrounding the blocks at the first sampling point (Fig. 5). Activity concentrations for the PFA:OPC and NRVB blends then approach input levels after 14 days. Transport through the Cebama reference blend is slower, taking 28 days to reach a C/C_0 value of 0.8 with CEM I and GGBS:OPC cements taking progressively longer; indeed, concentrations are apparently still increasing at the end of the experiment (270 days). On this basis, if technetium migration were to be unaffected by chemical interactions between solution and the cement solids, the rate of transport would be expected to decrease in the order PFA:OPC ≈ NRVB > Cebama ≫ CEM I ≈ GGBS:OPC (Fig. 5).

The findings for tritium are borne out with NRVB and, to an extent with PFA:OPC, though the latter displays more complex behaviour (Fig. 6). In the case of NRVB, ^{99}Tc appears in the surrounding solution after just one day, implying minimal retention. Levels reach a C/C_0 value above 0.7 after just one month and steady state is maintained at $C/C_0 = 0.8$ for the remainder of the experiment. Breakthrough also occurs rapidly with the PFA:OPC formulation; however, the peak in C/C_0 occurs after one month, followed by a slow and progressive decline (Fig. 6). This was unexpected and suggests that the ^{99}Tc released to solution is subsequently re-adsorbed or precipitated by the cement.

CEM I and GGBS:OPC gave similar profiles as for tritium, slowly increasing over 270 days, albeit at much lower C/C_0 values, (reaching only 0.2 and 0.3, respectively). Finally, measurements of ^{99}Tc activity in the solution surrounding the Cebama reference blend show no sign of breakthrough after 270 days (Fig. 7). This represents the most pronounced difference with tritium patterns (cf. Fig. 5) and the clearest indication of chemical retention displayed by all of the cements investigated in the study.

At the completion of the experiments, the blocks were cut longitudinally to reveal the centre of the cylinders, allowing the migration profile of ^{99}Tc to be examined from the central well to the outer edge of each block using digital autoradiography. Autoradiography of the NRVB reveals that the level of radioactivity within the cement is indistinguishable from background (Fig. 8a). This is in accordance with the solution analyses and demonstrates that this material has very little capacity to retain technetium. Autoradiographic images for CEM I and GGBS:OPC display broadly similar low levels of dispersed activity throughout the blocks (Fig. 8b and c), again consistent with migration of ^{99}Tc through the cement and a limited degree of retention. In the case of CEM I, the low level of radioactivity appears to be uniformly distributed, with the exception of a few small localised 'hot-spots' (Fig. 8b) that possibly correlate with discrete (dark) cement clinker particles. In the GGBS:OPC block, the distribution of radioactivity is more elevated in a diffuse band close to the wall of the central well, reaching a peak at a depth of 2–3 mm into the cement matrix. Thereafter, the activity gradually decreases to background levels towards the edge of the block (Fig. 8c).

Much greater retention of ^{99}Tc is apparent in both the Cebama reference blend and PFA:OPC cements. Autoradiography of the former (Fig. 9a) revealed a region of high activity close to the central well, with a very pronounced peak in activity at a depth of 1.5–2 mm into the cement, decreasing to background level between 9 and 10 mm from the well wall (features labelled 'y' in Fig. 9a(ii)). There is no evidence from autoradiography of ^{99}Tc transport further into the block, consistent with the solution analyses noted previously, where no breakthrough was observed into the surrounding solution with the Cebama reference blend. The autoradiographic images for PFA:OPC are interesting and point to more complex behaviour. Low-level activity from ^{99}Tc is present throughout the block and shows a generally decreasing trend from the central well to the surface (Fig. 9b). Superimposed on this trend is a narrow (<1 mm) zone of very high activity within the cement matrix peaking on, or within, 1 mm of the well wall (feature 'x'; Fig. 9b) beyond which activity levels fall rapidly over a distance of about 4 mm. Surprisingly, the zone of high ^{99}Tc enrichment occurs only to one side of the well (Fig. 9b(ii)), pointing towards disturbance of the sample during the experiment or a discontinuity, whether structural, mineralogical or chemical, in the sample. The autoradiography also shows that there is a significant amount of activity remaining within the well itself, which is also asymmetrically distributed to the same side of the well as the enrichment in the wall. This resembles some sort of gravitational sediment (or precipitate) deposition feature on this side of the cement block. The duplicate PFA:OPC sample was sectioned in order to investigate this

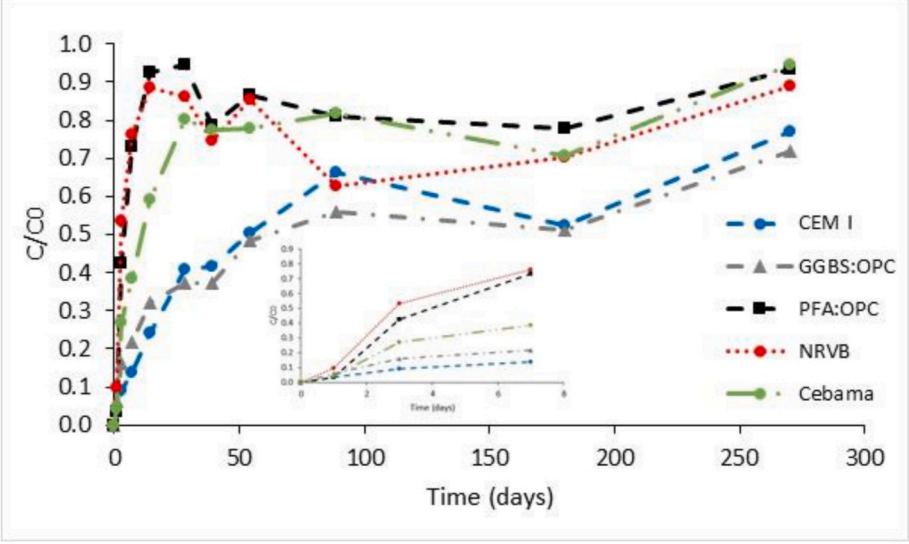

Fig. 5. Elution curves for tritiated water (HTO) in through-diffusion experiments. Insert shows changes over the first seven days.

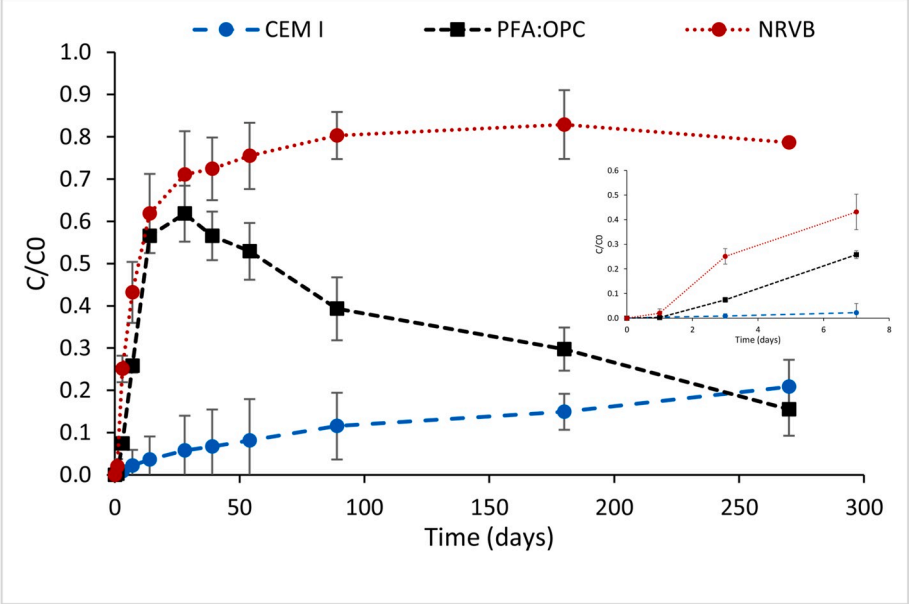

Fig. 6. Elution curves for ^{99}Tc in through-diffusion experiments on NRVB, CEM I and PFA:OPC. Insert shows changes over the first seven days.

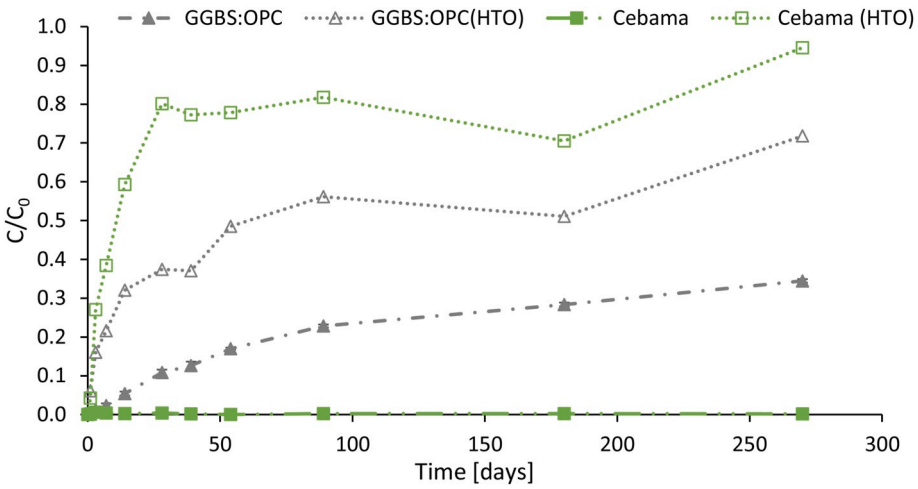

Fig. 7. Elution curves for ^{99}Tc in through-diffusion experiments on GGBS:OPC and Cebama reference blend with corresponding profiles for tritiated water (HTO).

apparent artefact; identical results were obtained (Fig. S3 in Supplementary Information).

The results above demonstrate that the capacity to retard technetium migration varies substantially among different cement formulations. The five HCP appear to fall into two distinct groups. The first displays conventional diffusive transport behaviour whereby the relative affinity of ^{99}Tc for the solid matrix increases from NRVB, through GGBS:OPC to CEM I. This results in chromatographic breakthrough into the solution surrounding the cement blocks and regular symmetrical profiles in the autoradiographs. It can be explained by reversible exchange of $^{99}TcO_4^-$ on C–S–H and AFm phases. Autoradiographs for the second group, comprising PFA:OPC and the Cebama reference blend, show high concentrations of Tc in narrow zones with limited evidence of further migration into the matrix. No breakthrough at all occurred for the Cebama reference blend, suggesting the *in situ* formation of a Tc-containing precipitate, probably due to reduction of Tc(VII) to Tc(IV). Although early breakthrough was observed for PFA:OPC, it decreased markedly over the course of the experiment. This apparently anomalous type of behaviour could be explained by the existence of a physical defect allowing fast transit that was subsequently blocked or, more plausibly, slower reaction kinetics for the precipitation process. Further work is required to characterise the zone of enhanced technetium uptake and identify the phase (or phases) responsible for immobilisation in these cement systems.

4. Conclusions

Batch experiments on individual mineral phases present in OPC and blended cements point to preferential but limited uptake of pertechnetate by pure (Fe-free) C–S–H and AFm, and no significant adsorption onto ettringite or calcium aluminates. The exchange process is rapid, reaching equilibrium in a few hours. Based on the distribution ratios determined for these phases and hardened cement pastes, technetium (VII) is expected to be mobile in cementitious materials, provided no reducing agents are present to promote precipitation in the form of Tc (IV). The results are borne out by through-diffusion tests on intact, monolithic cement blocks where markedly different migration rates and behaviour were observed, primarily due to chemical interactions with the cement matrix rather than differential permeability or other physical factors. A backfill cement, developed specifically for the purpose of

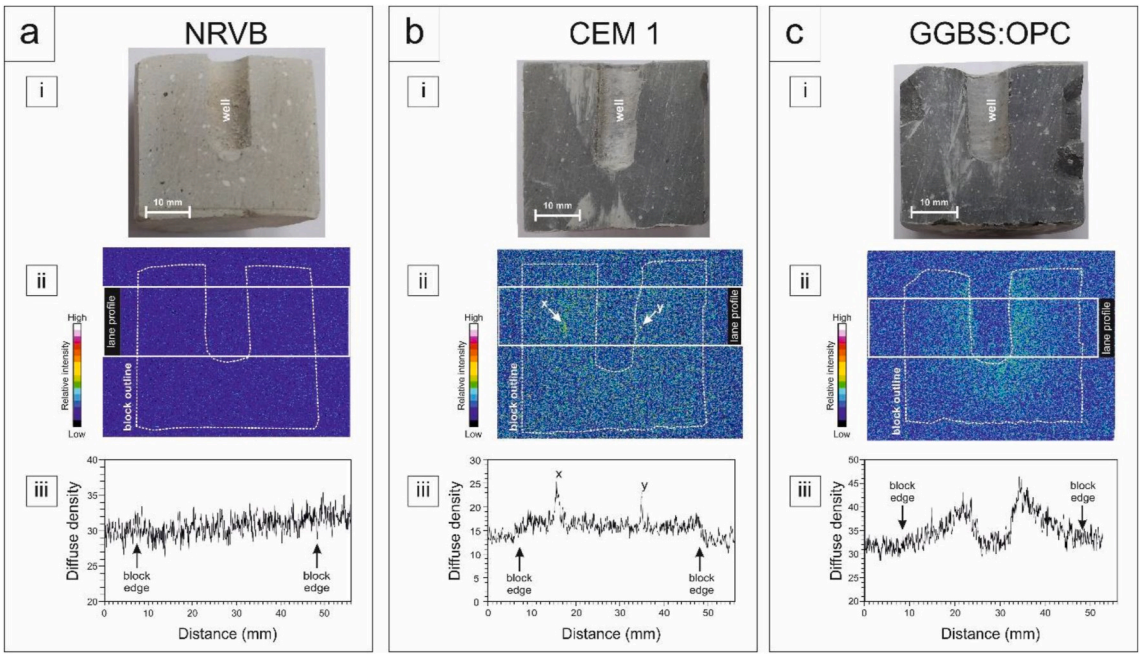

Fig. 8. LPSL autoradiography results for (a) NRVB, (b) CEM I and (c) GGBS:OPC. Each diagram shows: (i) a photograph of the longitudinally sawn surface of the cement block; (ii) corresponding 16-colour contoured linearised LPSL autoradiograph; (iii) profile of the variation in radioactivity across the block, measured along the 'lane' drawn in (ii). For CEM I (b), the locations of rare, discrete 'hots-spots' of radioactivity (labelled 'x' and 'y') are shown in the corresponding LPSL autoradiograph. (For interpretation of the references to colour in this figure legend, the reader is referred to the Web version of this article.)

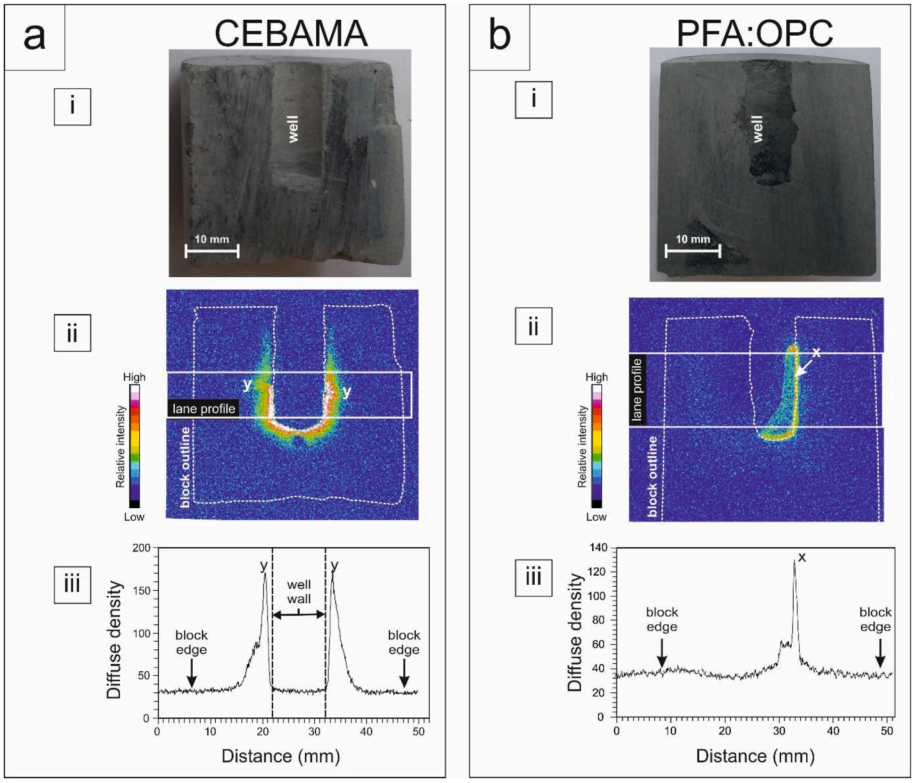

Fig. 9. LPSL autoradiography results for (a) Cebama reference blend and (b) PFA:OPC cement blocks. Each diagram shows: (i) photograph of the longitudinally sawn surface of the cement block; (ii) corresponding 16-colour contoured linearised LPSL autoradiograph; (iii) profile of the variation in radioactivity across the block, measured along the 'lane' drawn in (ii). In PFA-OPC (ii), radioactivity is concentrated only on one side of the well ('x'). In the Cebama reference blend block, the peak in radioactivity (y) is located within the cement and very close to the well wall. (For interpretation of the references to colour in this figure legend, the reader is referred to the Web version of this article.)

radionuclide retention (NRVB), gave by far the poorest performance of all formulations studied in terms of both transport rates and overall technetium retention. Two of the matrices, PFA:OPC and a low-pH blend incorporating fly ash, effectively retarded Tc migration via precipitation in narrow, reactive zones. The findings have important implications when choosing cementitious grouts and/or backfill for Tc-containing radioactive wastes.

Declaration of competing interest

The authors declare that they have no known competing financial interests or personal relationships that could have appeared to influence the work reported in this paper.

Acknowledgements

The research described in this paper has received funding from the European Union's Horizon 2020 Research and Training Programme of the European Atomic Energy Community (EURATOM) (H2020-NFRP-2014/2015) under grant agreement no 662147 (CEBAMA). We would like to thank Dr Marcus Altmaier of Forschungszentrum Karlsruhe and his colleagues for their invaluable support. Tapio Vehmas and Markku Leivo from VTT Technical Research Centre of Finland are acknowledged for providing samples and constituents of the Cebama low-pH reference cement paste. We would also like to acknowledge the help of colleagues in the Nuclear Metrology Group at the National Physical Laboratory, in particular Elsje van Es, Peter Ivanov and Lynsey Keighley.

Appendix A. Supplementary data

Supplementary data to this article can be found online at https://doi.org/10.1016/j.apgeochem.2020.104580.

References

Allen, P.G., Shuh, D.K., Bucher, J.J., Edelstein, N.M., Reich, T., Denecke, M.A., Nitsche, H., 1997a. Chemical speciation studies of radionuclides by XAFS. J. Phys. IV 7, 789–792.

Allen, P.G., Siemering, G.S., Shuh, D.K., Bucher, J.J., Edelstein, N.M., Langton, C.A., Clark, S.B., Reich, T., Denecke, M.A., 1997b. Technetium speciation in cement waste forms determined by X-ray absorption fine structure spectroscopy. Radiochim. Acta 76, 77–86.

Amersham Biosciences, 2005. *ImageQuant TL v.2005*. Amersham Biosciences. GE Healthcare Limited.

Angus, M., Borwick, J, Cann, G, 2011. The specification of cement powders for waste encapsulation processes at the Sellafield site. In: Proceedings of NUWCEM 2011, Avignon, France. INIS IAEA, Vienna, Austria, pp. 48–58.

Atkins, M., Glasser, F.P., Kindness, A., 1992. Cement hydrate phases: solubility at 25°C. Cement Concr. Res. 22, 241–246.

Atkins, M., Macphee, D., Kindness, A., Glasser, F.P., 1991. Solubility properties of ternary and quaternary compounds in the calcia-alumina-sulfur trioxide-water system. Cement Concr. Res. 21, 991–998.

Baur, I., Keller, P., Mavrocordatos, D., Wehrli, B., Johnson, C.A., 2004. Dissolution-precipitation behaviour of ettringite, monosulfate and calcium silicate hydrate. Cement Concr. Res. 34, 341–348.

Berner, U., 1999. Concentration limits in the cement based Swiss repository for long-lived, intermediate-level radioactive wastes (LMA). PSI Bericht, 99-10.

Bel, J.J., Wickham, S.M., Gens, R.M., 2006. Development of the Supercontainer design for deep geological disposal of high-level heat emitting radioactive waste in Belgium. Mater. Res. Soc. Symp. Proc. 932, 122.1.

Bonhoure, I., Scheidegger, A.M., Wieland, E., Dahn, R., 2002. Iodine species uptake by cement and C-S-H studied by I K-edge X-ray absorption spectroscopy. Radiochim. Acta 90, 647–651.

Brodda, B.G., Xu, M., 1989. Leaching of chlorine, cesium, strontium and technetium from cement-fixed intermediate level liquid waste. Mater. Res. Soc. Symp. Proc. 127, 481–487.

Brown, D.A., Chadwick, M.B., Capote, R., Kahler, A.C., Trkov, A., Herman, M.W., Sonzogni, A.A., Danon, Y., Carlson, A.D., Dunn, M., Smith, D.L., Hale, G.M., Arbanas, G., Arcilla, R., Bates, C.R., Beck, B., Becker, Brown, F., Casperson, R.J., Conlin, J., Cullen, D.E., Descalle, M.-A., Firestone, R., Gaines, T., Guber, K.H., Hawari, A.I., Holmes, J., Johnson, T.D., Kawano, T., Kiedrowski, B.C., Koning, A.J., Kopecky, S., Leal, L., Lestone, J.P., Lubitz, C., Marquez Damian, J.I., Mattoon, C.M., McCutchan, E.A., Mughabghab, S., Navratil, P., Neudecker, D., Nobre, G.P.A., Noguere, G., Paris, M., Pigni, M.T., Plompen, A.J., Pritychenko, B., Pronyaev, V.G., Roubtsov, D., Rochman, D., Romano, P., Schillebeeckx, P., Simakov, S., Sin, M., Sirakov, I., Sleaford, B., Sobes, V., Soukhovitskii, E.S., Stetcu, I., Talou, P., Thompson, I., van der Marck, S., Welser-Sherrill, L., Wiarda, D., White, M., Wormald, J.L., Wright, R.Q., Zerkle, M., Zerovnik, G., Zhu, Y., 2018. ENDF/B-VIII.0: the 8th major release of the Nuclear Reaction Data Library with CIELO-project cross sections, new standards and thermal scattering data. Nucl. Data Sheets 148, 1-142.

Bruno, J., Ewing, R.C., 2006. Spent nuclear fuel. Elements 2, 343–349.

Burke, I.T., Boothman, C., Lloyd, J.R., Mortimer, R.J.G., Livens, F.R., Morris, K., 2005. Effects of progressive anoxia on the solubility of technetium in sediments. Environ. Sci. Technol. 39, 4109–4116.

Carbol, P., Wegen, D.H., Wiss, T., Fors, P., 2012. Spent fuel as waste material. Compr. Nucl. Mater. 5, 389–420.

Childs, B.C., Poineau, F., Czerwinski, K.R., Sattelberger, A.P., 2015. The nature of the volatile technetium species formed during vitrification of borosilicate glass. J. Radioanal. Nucl. Chem. 306, 417–421.

Cathelin, R., 2012. *Linearize GelData*. Sigenae team, INTRA. Toulouse, France. http://imagej.nih.gov/ij/plugins/linearize-gel-data.html.

Corkhill, C.L., Bridge, J.W., Hillel, P., Gardner, L.J., Banwart, S.A., Hyatt, N.C., 2012. Technetium-99m transport and immobilisation in porous media: development of a novel nuclear imaging technique. Mater. Res. Soc. Symp. Proc. 1518, 123–129.

Cui, D., Eriksen, T.E., 1996. Reduction of pertechnetate in solution by heterogeneous electron transfer from Fe(II)-containing geological material. Environ. Sci. Technol. 30, 2263–2269.

Eriksen, T.E., Ndalamba, P., Cui, D., Bruno, J., Caceci, M., Spahiu, K., 1993. Solubility of the Redox-Sensitive Radionuclides ^{99}Tc and ^{237}Np under Reducing Conditions in Neutral to Alkaline Solutions. Effect of Carbonate. Svensk Kärnbränslehantering AB, Stockholm, Sweden, p. 32. SKB Technical Report, TR-93-18.

Evans, N.D.M., 2008. Binding mechanisms of radionuclides to cement. Cement Concr. Res. 38, 543–553.

Felipe-Sotelo, M., Hinchliff, J., Drury, D., Evans, N.D.M., Williams, S., Read, D., 2014. Radial diffusion of radiocaesium and radioiodide through cementitious backfill. Phys. Chem. Earth 70–71, 60–70.

Felipe-Sotelo, M., Hinchliff, J., Evans, N.D.M., Read, D., 2016a. Solubility constraints affecting the migration of selenium through the cementitious backfill of a geological disposal facility. J. Hazard Mater. 305, 21–29.

Felipe-Sotelo, M., Hinchliff, J., Field, L.P., Milodowski, A.E., Holt, J.D., Taylor, S.E., Read, D., 2016b. The solubility of nickel and its migration through the cementitious backfill of a geological disposal facility for nuclear waste. J. Hazard Mater. 314, 211–219.

Giffaut, E., Grivé, M., Blanc, Ph, Vieillard, Ph, Colàs, E., Gailhanou, H., Gaboreau, S., Marty, N., Madé, B., Duro, L., 2014. ANDRA thermodynamic database for performance assessment: ThermoChimie. Appl. Geochem. 49, 225–236.

Gilliam, T.M., Spence, R.D., Bostick, W.D., Shoemaker, J.L., 1990. Proceedings of the gulf coast hazardous substance research center second annual symposium: mechanisms and applications of solidification/stabilization of technetium in cement-based grouts. J. Hazard Mater. 24, 189–197.

Glasser, F.P., 2011. Application of inorganic cements to the conditioning and immobilisation of radioactive wastes. In: Ojovan, M.I. (Ed.), Handbook of Advanced Radioactive Waste Conditioning Technologies. Woodhead, pp. 67–135.

Gonzalez, A.L., Li, H., Mitch, M., Tolk, N., Duggan, D.M., 2002. Energy response of an imaging plate exposed to standard beta sources. Appl. Radiat. Isot. 57, 875–882.

Grambow, B., López-García, M., Olmeda, J., Grivé, M., Marty, N.C.M., Grangeon, S., Claret, F., Lange, S., Deissmann, G., Klinkenberg, M., Bosbach, D., Bucur, C., Florea, I., Dobrin, R., Isaacs, M., Read, D., Kittnerová, J., Drtinová, B., Vopálka, D., Cevirim-Papaioannou, N., Ait-Mouheb, N., Gaona, X., Altmaier, M., Nedyalkova, L., Lothenbach, B., Tits, J., Landesman, C., Rasamimanana, S., Ribet, S., 2020. Retention of radionuclides on cementitious systems: main outcome of the CEBAMA project. Appl. Geochem. (this issue).

Grivé, M., Duro, L., Colàs, E., Giffaut, E., 2015. Thermodynamic data selection applied to radionuclides and chemotoxic elements: an overview of the ThermoChimie-TDB. Appl. Geochem. 55, 85–94.

Hallam, R.J., Jain, S.L., Evans, N., 2011. Sorption of Tc(IV) to cementitious materials associated with a geological disposal facility for radioactive waste. In: Proc. Waste Management 2011 Conf (Phoenix, Arizona, USA).

Hawthorne, F.C., Krivovichev, S.V., Burns, P.C., 2000. The crystal chemistry of sulfate minerals. Rev. Mineral. 40, 1-112.

Hoch, A.R., Baston, G.M.N., Glasser, F.P., Hunter, F.M.I., Smith, V., 2012. Modelling evolution in the near field of a cementitious repository. Mineral. Mag. 76, 3055–3069.

Idiart, A. (Ed.), 2017. Preliminary Results and Interpretation of the Modelling of WP1 & WP2 Experiments, CEBAMA Deliverable D3.05, p. 70. http://www.cebama.eu/home/deliverables.

Isaacs, M., Hayes, M., Rawlinson, S., Angus, M., Qaisar, A., Christie, S., Edmondson, S., Read, D., 2018. The processing and product characteristics of a blended cement grout incorporating a polycarboxylate ether superplasticiser. Adv. Cement Res. 30, 148–158.

Jantzen, C., Johnson, A., Read, D., Stegemann, J., 2010. Cements in waste management. Adv. Cement Res. 22, 225–231.

Kim, D., Kruger, A.A., 2018. Volatile species of technetium and rhenium during waste vitrification. J. Non-Cryst. Solids 481, 41–50.

Kleykamp, H., 1988. The chemical state of fission products in oxide fuels at different stages of the nuclear fuel cycle. Nucl. Technol. 80, 412–422.

Lange, S., 2019. Structural Uptake and Retention of Safety Relevant Radionuclides by Cementitious Materials. PhD thesis. RWTH Aachen University.

Lange, S., Kowalski, P., Pšenička, M., Klinkenberg, M., Rohmen, S., Bosbach, D., Deissmann, G., 2018. Uptake of ^{226}Ra in cementitious systems: a complementary solution chemistry and atomistic simulation study. Appl. Geochem. 96, 204–216.

Leblans, P., Vandenbroucke, D., Willems, P., 2011. Storage phosphors for medical imaging. Materials 4, 1034–1086.

Lewis, B.J., Thompson, W.T., Iglesias, F.C., 2012. Fission product chemistry in oxide fuels. Compr. Nucl. Mater. 2, 515–546.

Lloyd, J., Sole, V., van Praagh, C., Lovley, D., 2000. Direct and Fe(II)-mediated reduction of technetium by Fe(II)-reducing bacteria. Environ. Microbiol. 66, 3743–3749.

Lukens, W.W., Shuh, D.K., Muller, I.S., McKeown, D.A., 2003. X-ray absorption fine structure studies of speciation of technetium in borosilicate glasses. Mater. Res. Soc. Symp. Proc. 802. DD3.3.1-DD3.3.6.

Luksic, S.A., Riley, B.J., Schweiger, M., Hrma, P., 2015. Incorporating technetium in minerals and other solids: a review. J. Nucl. Mater. 466, 526–538.

Ma, B., Fernandez-Martinez, A., Findling, N., Koishi, A., Tisserand, D., Bureau, S., Charlet, L., Grangeon, S., Tournassat, C., Claret, F., Marty, N.C.M., Salas-Colera, E., Elkaim, E., Marini, C., 2017. Evidence of multiple sorption modes in layered double hydroxides using Mo as structural probe. Environ. Sci. Technol. 51, 5531–5540.

Ma, B., Charlet, L., Fernandez-Martinez, A., Kang, M., Madé, B., 2019. A review of the retention mechanisms of redox-sensitive radionuclides in multi-barrier systems. Appl. Geochem. 100, 414–431.

Masters-Waage, N.K., Morris, K., Lloyd, J.R., Shaw, S., Mosselmans, J.F.W., Boothman, C., Bots, P., Rizoulis, A., Livens, F.R., Gareth, T.W., Law, G.T.W., 2017. Impacts of repeated redox cycling on technetium mobility in the environment. Environ. Sci. Technol. 51, 14301–14310.

Matschei, T., Lothenbach, B., Glasser, F.P., 2006. The AFm phase in Portland cement. Cement Concr. Res. 37, 118–130.

Mattigod, S.V., Whyatt, G.A., Serne, R.J., Martin, P.F., Schwab, K.E., Wood, M.I., 2001. Diffusion and Leaching of Selected Radionuclides (Iodine-129, Technetium-99, and Uranium) through Category 3 Waste Encasement Concrete and Soil Fill Material. Pacific Northwest National Laboratory (PNNL), PNNL-13639. Richland, WA (United States).

Mattigod, S.V., Whyatt, G.A., Serne, J.R., Wood, M.I., 2004. Diffusion of iodine and technetium-99 through waste encasement concrete and unsaturated soil fill material. Mater. Res. Soc. Symp. Proc. 824, 391–398.

Milodowski, A.E., Rochelle, C.A., Purser, G., 2013. Uptake and retardation of Cl during cement carbonation. Procedia Earth Planetary Sci 7, 594–597.

NAGRA, 2002. Project Opalinus Clay - Safety Report. Demonstration of Disposal Feasibility for Spent Fuel, Vitrified High-Level Waste and Long-Lived Intermediate-Level Waste (Entsorgungsnachweis). NAGRA Technical Report 02-05, Wettingen.

NAGRA, 2008. Entsorgungsprogramm 2008 der Entsorgungspflichtigen. NAGRA Technischer Bericht 08-01. Wettingen.

Ochs, M., Mallants, D., Wang, L., 2016. Radionuclide and Metal Sorption on Cement and Concrete. Springer, p. 301.

Pegg, I.L., 2015. Behavior of technetium in nuclear waste vitrification processes. J. Radioanal. Nucl. Chem. 305, 287–292.

Posiva, 2012. Safety Case for the Disposal of Spent Nuclear Fuel at Olkiluoto. Posiva Report 2012-12.

Rasband, W.S., 2013. ImageJ v.1.48k (15 December 2013. US National Institutes of Health, Bethesda, Maryland, USA, 1997-2016. http://rsb.info.nih.gov/ij.

Saslow, S.A., Um, W., Russell, R.L., Williams, B.D., Assmussen, R.M., Varga, T., Qafoku, O., Riley, B.J., Lawter, A.R., Snyder, M.M.V., Baum, S.R., Leavy, I.I., 2018. Effluent Management Facility Evaporator Bottoms: Waste Streams Formulation and Waste Form Qualification Testing. Pacific Northwest National Lab. (PNNL), PNNL-26570. Richland, WA (United States).

Schulte, E., Scoppa, P., 1987. Sources and behaviour of technetium in the environment. Sci. Total Environ. 64, 163–179.

SKB, 2015. Safety Analysis for SFR Long-Term Safety: Main Report for the Safety Assessment SR-PSU. Svensk Kärnbränslehantering AB.

Shannon, R.D., 1976. Revised effective ionic radii and systematic studies of interatomic distances in halides and chalcogenides. Acta Crystallogr. A 32, 751–767.

Smith, R.W., Walton, J.C., 1993. The role of oxygen diffusion in the release of technetium from reducing cementitious waste forms. Mater. Res. Soc. Symp. Proc. 294, 247–253.

Tallent, O.K., McDaniel, E.W., Cul, G.D.D., Dodson, K.E., Trotter, D.R., 1987. Immobilization of technetium and nitrate in cement-based materials. Mater. Res. Soc. Symp. Proc. 112, 23–32.

Takahashi, K., 2002. Progress in science and technology on photostimulable BaFX:Eu^{2+} (X=Cl, Br, I) and imaging plates. J. Lumin. 100, 307–315.

van Es, E., Hinchliff, J., Felipe-Sotelo, M., Milodowski, A.E., Field, L.P., Evans, N.D.M., Read, D., 2015. Retention of chlorine-36 by a cementitious backfill. Mineral. Mag. 79, 1297–1305.

Vehmas, T., Montoya, V., Cruz Alonso, M., Vašíček, R., Rastrick, E., Gaboreau, S., Večerník, P., Leivo, M., Holt, E., Ait Mouheb, N., Finck, N., Schild, D., Schäfer, T., Adam, C., Dardenne, K., Rothe, J., Fernandez, A., Garcia-Calvo, J.L., Felipe-Sotelo, M., Svoboda, J., Isaacs, M., Read, D., Červinka, R., Rosendorf, T., Vasconcelos, R., Provis, J., Hyatt, N., Corkhill, C., 2020. Slag containing low-pH cementitious materials for deep underground nuclear waste repositories. Appl. Geochem. 112.

Vehmas, T., Schnidler, A., Löija, M., Leivo, M., Holt, E., 2017. Reference mix design and castings for low-pH concrete for nuclear waste repositories. KIT Sci. Rep. 7734, 101–111.

Verhoef, E.V., de Bruin, A.M.G., Wiegers, R.B., Neeft, E.A.C., Deissmann, G., 2014. Cementitious Materials in OPERA Disposal Concept in Boom Clay. Report OPERA-PG-Cov020. COVRA, Vlissingen.

Warwick, P., Aldridge, P., Evans, N., Vines, S., 2007. The solubility of technetium (IV) at high pH. Radiochim. Acta 95, 709–716.

Weaver, J., Soderquist, C.Z., Washton, N.M., Lipton, A.S., Gassman, P.L., Lukens, W.W., Kruger, A.A., Wall, N.A., McCloy, J.S., 2017. Chemical trends in solid alkali pertechnetates. Inorg. Chem. 56, 2533–2544.

Westsik Jr., J, Cantrell, K, Serne, R, Qafoku, N, 2014. Technetium Immobilization Forms: Literature Survey, , EMSP-RPT-023PNNL-23329. US DoE.

Wieland, E, Tits, J, Spieler, P, Dobler, J, 1998. Interaction of Eu(III) and Th(IV) with sulfate-resisting portland cement. Mater. Res. Soc. Symp. Proc. 506, 573–578.

Wildung, R., McFadden, K., Garland, T., 1978. Technetium sources and behaviour in the environment. J. Environ. Qual. 8, 156–161.

Zeissler, C.J., 1997. Comparison of semiconductor pixel array, phosphor plate, and track-etch detectors for alpha autoradiography. Nucl. Instrum. Methods Phys. Res. A392, 249–253.